Modeling the Chandra Space Environment

W.C. Blackwell, Jr.*[a], J.I. Minow[a], S.L. O'Dell[b], R.M. Suggs[b], D.A. Swartz[c], A.F. Tennant[b], S.N. Virani[d], and K.M. Warren[e**]

[a]Sverdrup Technology, Inc., Marshall Space Flight Center Group, Huntsville, AL 35806
[b]NASA Marshall Space Flight Center, Huntsville, AL 35812
[c]Universities Space Research Association, NASA/MSFC, Huntsville, AL 35812
[d]Harvard-Smithsonian Center for Astrophysics, Cambridge, MA 02138
[e]Raytheon ITSS, MSFC, Huntsville, AL 35812

ABSTRACT

This paper describes the development of CRMFLX, an ion model for the outer magnetosphere developed for scheduling periods when the Advanced CCD Imaging Spectrometer (ACIS) instrument onboard the *Chandra* X-ray Observatory can be safely moved into the focal plane position required for science observations. Because exposure to protons with energies of approximately 100 keV to 200 keV has been shown to produce an increase in the charge transfer inefficiency (CTI) of the ACIS instrument, a tool for predicting encounters with magnetospheric regions rich in these particles is required. The model is based on data from the EPIC/ICS instrument onboard the *Geotail* satellite and provides the user with flux values for 100 kev to 200 keV protons as a function of satellite position and the geomagnetic activity Kp index.

Keywords: *Chandra* X-Ray Observatory, protons, environment, magnetotail, magnetosheath, solar wind, ACIS, degradation

1. INTRODUCTION

The successful launch and deployment of the *Chandra* X-ray Observatory (CXO) provided a new and important tool for astronomical observations at x-ray wavelengths. The scientific program has been impacted by the post-launch discovery of space environment related damage to the Advanced CCD Imaging Spectrometer (ACIS) detector. A reduction in the resolving power of the front-illuminated CCD components was discovered early in the mission when it was determined that exposure to the space environment during passages through the radiation belts led to the damage. Investigation into the source of the sensor degradation showed that 100 keV to 200 keV protons (or possibly heavier ions with energies between approximately 200 keV and 1 MeV) scatter from the grazing incidence optics and impact the ACIS detector when it is in the focal plane position required for science observations.[1,2] The lattice displacement damage in the sensitive area of the CCD charge-transfer channel leads to a reduction in the efficiency of charge transfer from the CCD.[3,4] An increase of charge transfer inefficiency (CTI) in reading electrons from the CCD during the *Chandra* mission will lead to loss of image resolution in one of the more important sensors onboard the *Chandra* X-Ray Observatory. While it is desirable to optimize the science observing time, use of the ACIS detector at any point along its orbit will entail risk of exposure to potentially damaging proton flux. A strategy must be adopted that will result in successful science operations but will ensure the ACIS detector is moved out of the focal plane when the satellite is in regions of space where the flux of 100 keV ions is too large to permit safe operation. The strategy adopted by the *Chandra* team is to target a CTI increase of 5% CTI increase per year for a total CTI increase of 50% over a ten year mission lifetime. Scheduling the use of ACIS with these guidelines will assure successful ACIS science operations for the duration of the CXO mission.

Protons with energies of 100-200 keV are present throughout the region of space traversed by the *Chandra* orbit. The large eccentricity of the orbit, ~2.5 geocentric Earth radii (R_E) at perigee and 22.7 R_E at apogee, causing the satellite to sample a wide range of magnetospheric plasma regimes as well as the magnetosheath and solar wind. The radiation belts contain proton fluxes in excess of the threshold identified as dangerous to the detector. Indeed, early in the mission it was determined that the ion flux encountered in the ring currents inside radial distances of 2 R_E to 7 R_E are too large to safely use the ACIS instrument. Even at distances beyond geosynchronous orbit episodic injections of plasma from the magnetotail during substorms and major

---

*Correspondence: Email: bill.blackwell@msfc.nasa.gov; Telephone: 256 544 6741; Fax: 256 544 0242
**Now at Johns Hopkins University, Applied Physics Laboratory, Laurel, Maryland, 20723.

X-Ray and Gamma-Ray Instrumentation for Astronomy XI, Kathryn A. Flanagan, Oswald H. W. Siegmund, Editors, Proceedings of SPIE Vol. 4140 (2000) © 2000 SPIE · 0277-786X/00/$15.00

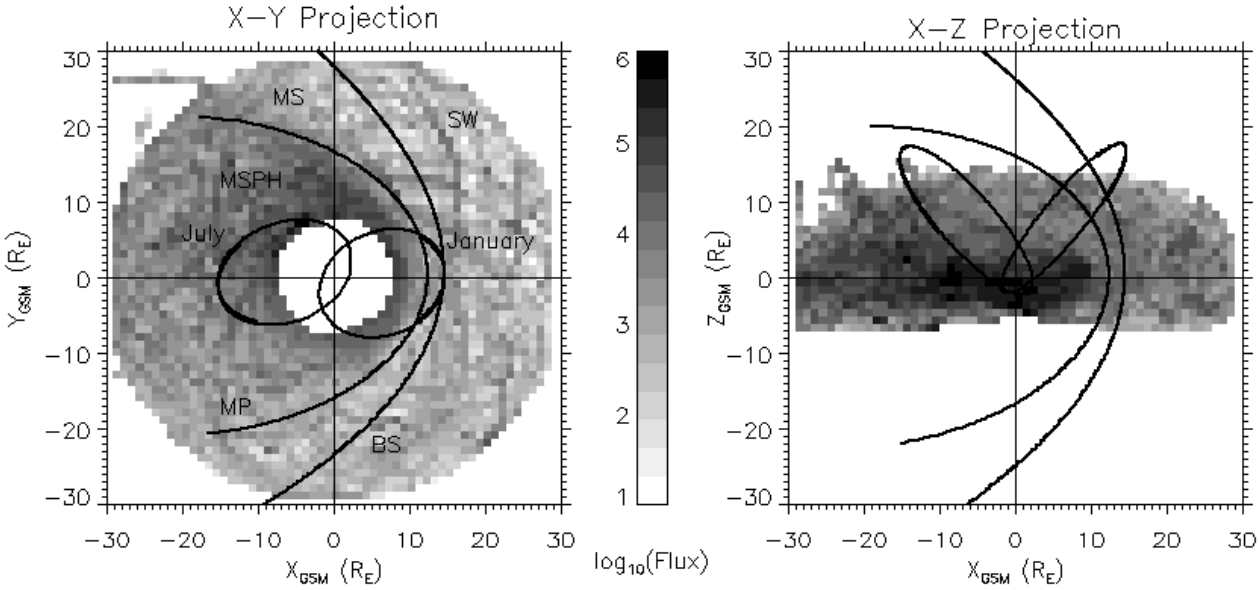

Figure 1. Geotail EPIC/ICS Proton Data. Average flux (protons/[cm^2-sec-sr-MeV]) from the P3 and P4 proton channels for all data from 1995 through 2000 are projected onto the GSM X-Y and X-Z planes. The Sun is to the right (positive X_{GSM} values) and the magnetotail to the left (negative X_{GSM} values). Nominal positions of the magnetopause (MP) and bow shock (BS) from Fairfield et al.[5] are indicated. The magnetosphere (MSPH) is the region inside the MP, the magnetosheath (MS) is bounded by the MP and BS, and the solar wind (SW) lies outside the BS.

magnetic storms may increase proton fluxes by orders of magnitude. Although reduced in flux, 100-200 keV protons are also found outside of the magnetosphere in the dusk and dayside magnetosheath, or even upstream of the bow shock, because "leakage" across the magnetopause is one of the loss mechanisms for magnetospheric plasma.[6,7] Energetic solar protons are an additional source of damaging particles, which increase the risk to the ACIS detector when the satellite is in the solar wind, magnetosheath, or outer magnetosphere.

An example of the variety of plasma regimes sampled by the satellite over the course of a year is shown in Figure 1. The CXO orbit is nearly fixed in inertial space over the course of year while the orientation of the magnetosphere is aligned with the sun. CXO passes through various regions of the magnetosphere throughout the year since the magnetosphere is changing orientation in inertial space due to the orbit of the Earth about the Sun. Orbits 6 months apart in both the X-Y and X-Z GSM planes are indicated in the figure. The orbit with primarily positive X_{GSM} values is for the period from January 15 through 18, 2000 when the satellite samples the dayside region of the magnetosphere. An orbit from 6 months later, 13 through 16 July 2000, shows the satellite inside the magnetosphere throughout the entire orbit.

A number of strategies are available to assure the safe use of the ACIS instrument. The current strategy for determining when the ACIS detector may be placed in the focal plane position required for science observations is based on estimates of ion flux from the AP-8 ion model.[8,9] A conservative strategy adopted by the *Chandra* team is to "safe" the ACIS detector (move it out of the focal plane position where it is exposed to the ion environment to a location protected from damaging protons) some period of time (10,000 seconds at the time of writing) before entering the radiation belts. The detector is not currently used for radial distances less than approximately 12 R_E from the Earth due to this strategy. In addition, if the Electron, Proton, and Helium Instrument onboard the spacecraft detects particle fluxes greater than a critical threshold adopted by the *Chandra* team, ACIS observations are automatically stopped and the detector moved out of the focal plane position[10]. Solar proton flux is available from the Advanced Composition Explorer satellite in near real-time to warn of solar proton events as well. In order to correctly assess the impact of ion populations in the outer magnetosphere on the operation of ACIS, a higher fidelity proton model is required that includes the asymmetric distribution of protons in the magnetosphere that will adequately predict the points in space and time along the *Chandra* orbit with significant fluxes of 100-200 keV protons.

Table 1. *Geotail* EPIC/ICS Energy Bands

Channel Name	Species	Energy Band (kev/e)**	Sector (deg)	Time Res.[a] (sec)	Time Res. Database[b] (min)
P4	p+	107.4 - 154.3	22.5	48	4.8
P5	p+	154.3 - 227.5	22.5	48	4.8
HE4	He	135.0 - 194.0	22.5	48	4.8
HE5	He	194.0 - 280.8	22.5	48	4.8
HE6	He	280.8 - 407.4	22.5	48	4.8
M5	CNO	360.2 - 493.5	22.5	48	4.8
M6	CNO	493.5 - 697.2	22.5	48	4.8
M7	CNO	697.2 - 1016.2	22.5	96	4.8

[a]Time resolution of original data.
[b]Time resolution of spin averaged data obtained from Principle Investigator.

The AP-8 flux model currently used in the off-line system (OFLS) on-orbit event scheduling software to predict radiation belt entry and exit times is useful to indicate the boundaries of the trapped, energetic particles in the proton radiation belts but is less useful for the lower energy ions in the outer magnetosphere due to two significant limitations of the model. AP-8 is only valid over radial distances of approximately 1.15 R_E to 6.6 R_E (c.f., Fung[11]) and proton spectra for energies less than about 10 MeV are the result of interpolation from higher energies so that use of the model for energies near 100 keV is not advised for applications requiring accurate ion flux values.[12] Indeed, analysis of the applicability of the AP-8 software for the *Chandra* problem by Virani et al.[10] demonstrated the code is often not adequate for providing even the MeV proton flux boundaries required to predict radiation belt entry and exit times. The AP-8 model is certain to produce even greater errors in the outer magnetosphere at energies of a few hundred keV since ion fluxes in this energy range are not azimuthally symmetric as the AP-8 model assumes.

The *Chandra* team requires an ion model for rapidly estimating the flux of 100 keV to 200 keV protons and heavier ions with energies of a few hundred keV as a function of geomagnetic disturbance over the entire CXO orbit at distances typically beyond 9 Re – 10 Re. The code must correctly model the dawn-dusk ion flux asymmetry observed in outer magnetosphere ion populations at the hundred of keV energies and must depend on the level of geomagnetic activity to provide estimates of proton flux during geomagnetic storms as well as to estimate fluence for scheduling observations for intervals up to a few weeks in the future.

To meet this requirement it was decided to develop an empirical engineering model based on satellite observations. Our approach is to create a database driven model that provides the free field ion flux (i.e., outside of the spacecraft) of interest to CXO. Two versions of the model are required, an average model that can be used to schedule observations for weeks in advance and a dynamic model driven by geomagnetic indices to be used to estimate fluxes in near real time. The average model is to be incorporated into the CXO off-line mission planning system (OFLS) to aid in the determination of times the ACIS detector can be safely used in the focal plane position. The primary use for the new code is to assess the ion fluence at 100-200 keV for individual orbits and provide a tool to manage the ACIS CTI degradation over the lifetime of the mission.

2. INSTRUMENTATION AND DATA ANALYSIS

The data used to construct the model is obtained from the Ion Composition Subsystem (ICS) of the Energetic Particles and Ion Composition (EPIC) instrument onboard the *Geotail* spacecraft.[13] *Geotail* was launched in 1992 and was primarily a deep tail mission for the first years of its operation. In early 1995 the satellite orbit was changed to a 30 x 9 Re orbit providing good coverage of the outer magnetosphere near the Earth. Data from January 1995 through February 2000 obtained from the Applied Physics Laboratory at Johns Hopkins University (JHU/APL) provided an extensive database for deriving the model. The satellite spins at a rate of approximately 20 rpm with the spin axis 87 degrees to the ecliptic plane. EPIC/ICS samples

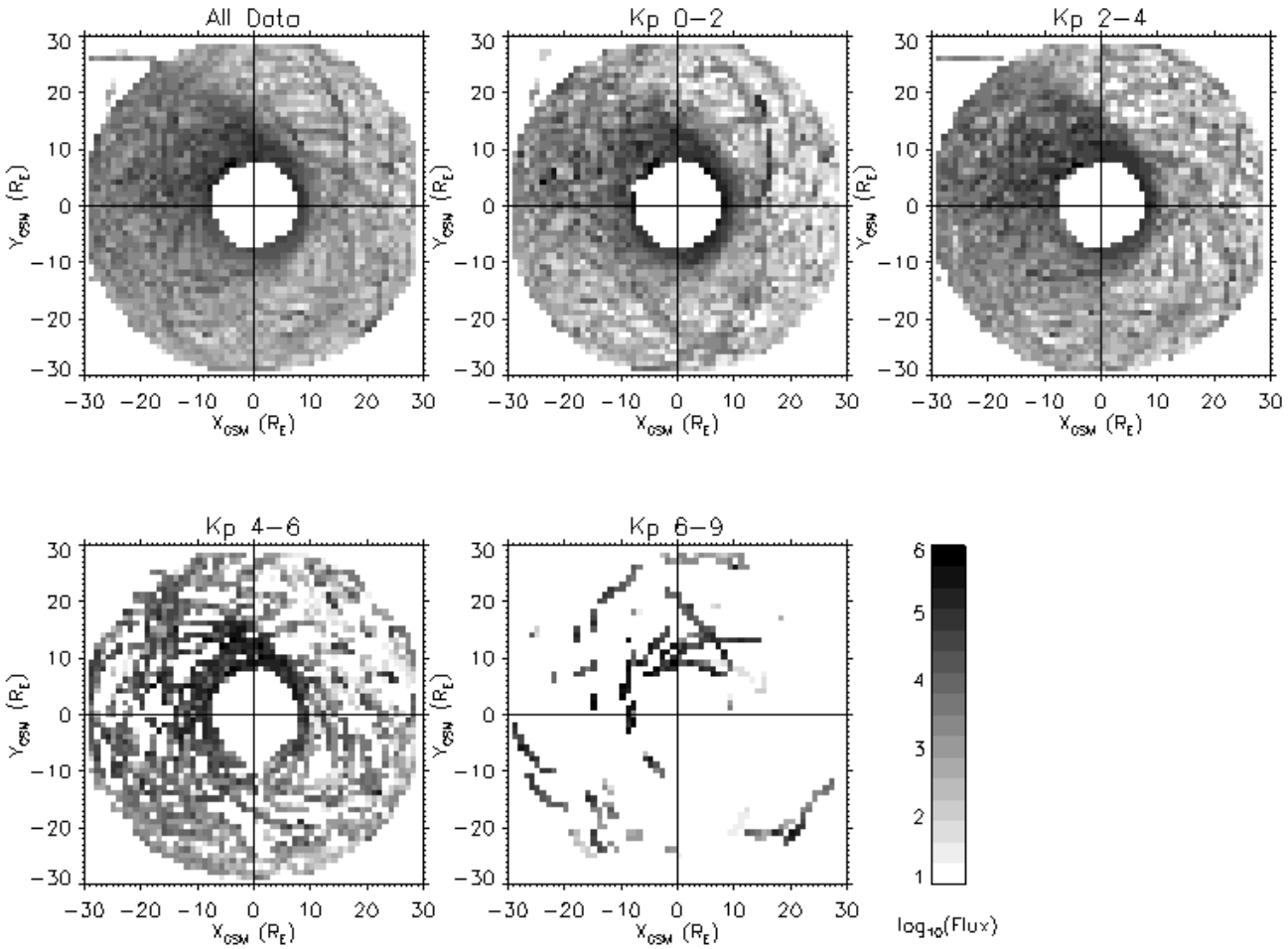

Figure 2. Proton Database as a Function of Kp. Average of all the data for the period 1995 through 2000 is given first in the upper left while the data is binned according to Kp in the rest of the plots. Note that the Kp 2-4 plot is most similar to the average, although Kp distributions typically exhibit a peak in the 1-2 range, because there are orders of magnitude flux at greater Kp values dominating the average. Flux units are protons/[cm^2-sec-sr-MeV].

nearly perpendicular to the spin axis or near the ecliptic plane. Original EPIC records of flux in 22.5-degree azimuthal sectors at 48-second time resolution are accumulated for approximately 4.8 minutes and the resulting values averaged. Ion mass and energy over a range of energies from 50 keV to 3 MeV are available from the EPIC/ICS instrument. Table 1 lists the channels of interest to ACIS. The P4 (107.4—154.3 keV) and P5 (154.3—227.5) channels approximately cover the 100-200 keV range of interest for the proton damage and the additional energy bands for the He and CNO instruments are available should these species be identified as important at a later time. The heavy ion species are also included in the database since it is not currently certain what their impact may be on the ACIS detector. The channels listed are consistent with the energies of heavy ions capable of scattering from the mirrors and depositing energy in the gate structure of the CCDs.

EPIC/ICS H, He, and CNO data files were calibrated by the Principal Investigator and provided in the form of time tagged flux records in units of ion/[cm^2-sec-sr-keV]. Spatial ordering of the time tagged records was performed by using *Geotail* ephemeris files interpolated to the flux observations times, producing intermediate time tagged files of flux and three dimensional location in space. Each data record was also tagged with the Kp index appropriate for the 3 hour Kp interval in which the measurement occurred. An intermediate set of data files for each year from 1995 through 2000 were created that contained the time tagged flux, spacecraft location, and Kp index. Figure 2 shows the data binned in levels of increasing geomagnetic activity as indicated by the Kp index as well as an average of all the flux in the database.

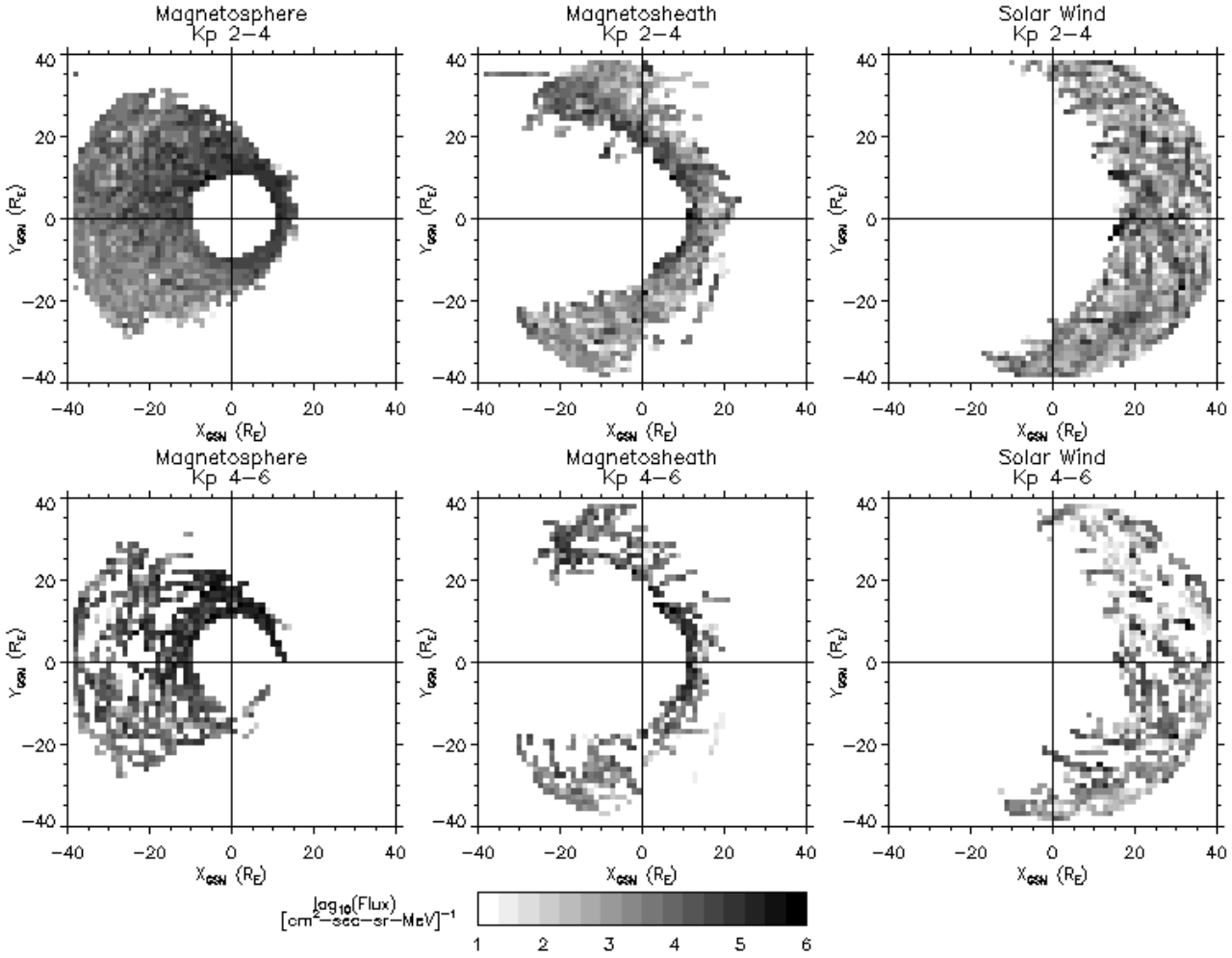

Figure 3. Plasma Region Identification. Flux values in the magnetosphere are greater for the larger Kp values and cover a wider range of local times in the midnight sector. The shift in the magnetopause from ~15 Re in the Kp 2-4 case to ~12 Re in the Kp 4-6 case reflects the correlation between geomagnetic disturbances and increased solar wind dynamic pressure which drives the magnetopause Earthward.

Ion flux records were also identified with an index indicating the phenomenological plasma region in which the record was obtained. Each record was identified as being solar wind, magnetosheath, or magnetosphere. The intent was to assure that subsequent processing of the records maintained the identify of the particles to avoid averaging solar wind with magnetosheath, magnetosheath with magnetosphere, etc. Identification of the plasma regime cannot be accomplished with only the EPIC/ICS data so a better indicator was required. Ion and electron spectrograms from the Comprehensive Plasma Instrument (CPI) Hot Plasma Analyzer (HPA) on *Geotail* provided the region identification.[14] For the purposes required here, it was adequate to use the 5 day survey plots provided by the CPI Principal Investigators on their web site (http://www-pi.physics.uiowa.edu/cpi-data/survey) to categorize each EPIC/ICS record as solar wind, magnetosheath, and magnetosphere based on energy, temperature, and flux characteristics of the individual plasma regimes. Data from ambiguous boundary crossings or during dynamic periods where numerous magnetopause or bow shock crossings were indicated are not included in the database.

Figure 3 gives examples of the proton database divided into individual plasma regions, for a range of Kp values from 2 to 4 and from 4 to 6 are given in. Magnetospheric populations of the 100 keV to 200 keV protons typically exhibit greater fluxes than those found in the in the magnetosheath and solar wind, consistent with the magnetospheric source of the 100 – 200 keV ions. Enhanced ion flux regions do occur in isolated locations in the solar wind. The most likely source of these particles are solar proton events since no attempt was made to remove transient energetic solar fluxes from the database. An asymmetry is also noted in the magnetosheath flux, particularly in the Kp 4 – 6 plot. Greater fluxes are observed near the magnetopause in the

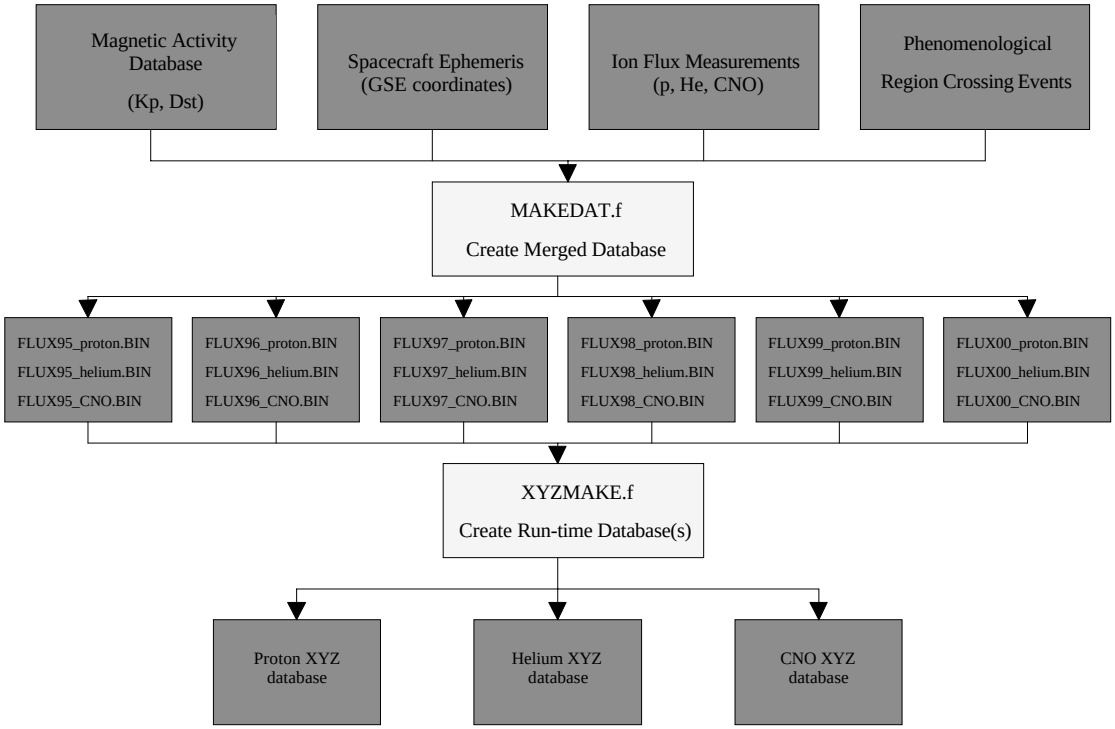

Figure 4. Schematic of Process Required to Create the Ion Flux Database. Time tagged ion flux measurements and ephemeris records from the EPIC/ICS instrument along with geomagnetic indices (Kp, Dst) and identification of the plasma regimes (solar wind, magnetosheath, or magnetosphere) are combined to create a merged database for individual years. This database is then processed into individual runtime databases of ion flux (proton, helium, or CNO).

dusk sector than in the dawn sector. These particles are due to "leakage" fluxes from the magnetosphere, ions drifting into the dusk sector which encounter the magnetopause and are lost from the magnetosphere.[7] Finally, there is a suggestion of an asymmetry in the solar wind fluxes for both the low (Kp 2-4) and high (Kp 4-6) geomagnetic activities as well. Flux values for $Y_{GSM}<0$ appear to include more large flux values than the $Y_{GSM}>0$ region. This asymmetry is consistent with spatial distribution of ions lost from the magnetosphere into the magnetosheath[15] and upstream from the Earth's bow shock in the solar wind.[16]

An overview of the complete process of producing the ion flux databases is provided in the schematic in Figure 4. Note that while only the proton results are presented here parallel development of helium and CNO databases are also included in the model. It is not certain at this time the possible impact on the ACIS CCD's of the heavy ions but capability is being built into the model should evidence arise that these species are a significant cause of concern.

3. CRMFLX ION MODEL

CRMFLX is the model of ion flux as a function of the spacecraft's location and the magnetic activity Kp index providing estimates of the mean, 50%, and 95% level ion flux environments over a radial distance from 9 R_E to 30 R_E from the center of the Earth. The code contains three separate ion flux models for the solar wind, magnetosheath, and magnetosphere. The first function performed by the model is a determination of which phenomenological region in which the spacecraft resides for a given location in space and geomagnetic activity index. The spacecraft's coordinates in the Geocentric Solar Magnetic (GSM) coordinate system are transformed into a system aligned with the magnetotail to account for the aberration angle due to the Earth's motion through the solar wind. CRMFLX incorporates code from two space environment models to calculate the magnetopause and bow shock boundary locations. The magnetopause boundary model is taken from the latest version of the Tsyganenko geomagnetic field model.[17,18] This is a relatively simple model, with the dynamic pressure being the only solar

wind parameter required as input. The bow shock model used in CRMFLX is adapted from a model developed by Bennett et. al.[19] The inputs to the Bennett bow shock model are more extensive than for the magnetopause model. The Cartesian components of the interplanetary magnetic field (IMF) vector, components of the solar wind bulk flow velocity vector, the solar wind's proton number density, the helium fraction of the solar wind ions, and temperatures of each component of the solar wind plasma (proton, electron, and helium) are all required input to the Bennett et al code. Exercising the models with a wide range of input parameters determined the best fit magnetopause and bow shock boundaries to the database boundaries as a function of Kp for ranges of Kp=0-2, 2-4, 4-6, and 6-9. The current value of the Kp index is used as an input to CRMFLX to determine which set of solar wind conditions are to be used to drive the magnetopause and bow shock boundary location calculations when running the model.

The current version of the code assumes the ion flux in the magnetosheath and solar wind are spatially uniform but vary as a function of Kp. The magnitude of the magnetosheath flux is an average of all ion database records identified as magnetosheath for a given Kp level at mean, 50%, and 95% flux levels. Similarly, an average of all database values identified as solar wind for a given Kp value is used for the magnitude of the solar wind ion flux. We anticipate including spatial variations in the magnetosheath and solar wind in future versions of the code. Although the Kp index is related to currents flowing in the mid-latitude ionosphere[20] and not really a measure of variation in interplanetary plasma conditions, Kp does correlate with the solar wind speeds since high velocity flows couple more energy into the magnetosphere driving geomagnetic disturbances. There is therefore an effective variation with Kp in parameters such as the solar wind dynamic pressure and particle flux in the solar wind and magnetosheath. Additional functionality is provided in the code to use other satellite data (for example from upstream monitors near L2) to specify solar wind and magnetosheath proton flux.

Spacecraft locations inside the magnetopause use the CRMFLX magnetosphere spatially dependent flux model. The ion flux environment inside the magnetosphere is highly variable in space, making these calculations more involved than in the case for either the solar wind or the magnetosheath. In CRMFLX, the approach taken for the magnetosphere region is to use the ion database described in the previous section to derive a spatially dependent flux model. The magnetosphere's database consists of a series of volume elements (1 R_E x 1 R_E x 1 R_E) which contain the average value for the ion flux in that region of space. Each volume element has the average flux stored separately in nine individual Kp intervals (Kp=0-1, 1-2, … , 7-8, 8-9). The data sampling at the higher Kp values is poor, so a given database volume element will typically contain average flux values for only a subset of the Kp intervals. Each volume element's data record also contains the number of measurements in each Kp interval.

Flux measurements are sparse at large Kp (Kp > 6) values over much of the magnetosphere as shown in Figure 2 and 3, requiring a spatial sector Kp scaling approach to extend the model to larger Kp values. Scaling laws are used which govern the scaling of the average flux at a given Kp value to the mean, 50%, and 95% levels for any valid Kp value. A number of spatial sectors were chosen (11 in the current model) so that Kp scaling laws could be derived that cover the entire range of Kp values, while having spatial locations dispersed throughout the magnetosphere. This process is shown in Figure 5a where sector locations are identified in a projection of the proton database on the X-Y_{GSM} plane. An example of the 50%, mean, and 95% flux is plotted in Figure 5b for Sector 2 as a function of Kp. The series of curves drawn through the data points indicate the fits used to derive the scaling laws. For each sector in 5a there are unique scaling laws used to determine how the flux varies as a function of Kp. The ion flux Kp scaling parameters for each spatial sector are recalculated only if the Kp value has changed by more than a predetermined tolerance value (currently set to 0.3 Kp) for computational efficiency. This is a reasonable assumption since Kp is typically a slowly varying parameter, varying on 15 minute or three hour time scales depending on the source of the records.

Flux is noted to increase with increasing Kp up to Kp=6 where the flux begins to decrease. The likely explanation for this behavior of the data lies in the nature of the Kp index. Magnetometer records at a series of mid-latitude sites are used to obtain the index. The maximum deviation of the magnetometer record in the three-hour Kp interval is used to produce the index for that interval (c.f., Mayaud[20]). If, for example, it is quiet for the first two hours and most of the third hour but a large disturbance is observed before the next Kp interval, then the entire interval is tagged with the large Kp, even though most of the data during the interval is appropriate for the quiet (low Kp) conditions. Due to the relatively low number of extreme Kp values in our data set we are subject to poor statistics and problems in incorporating the data sets. We have assumed for the results shown here that the flux increases with increasing Kp and determined the flux accordingly.

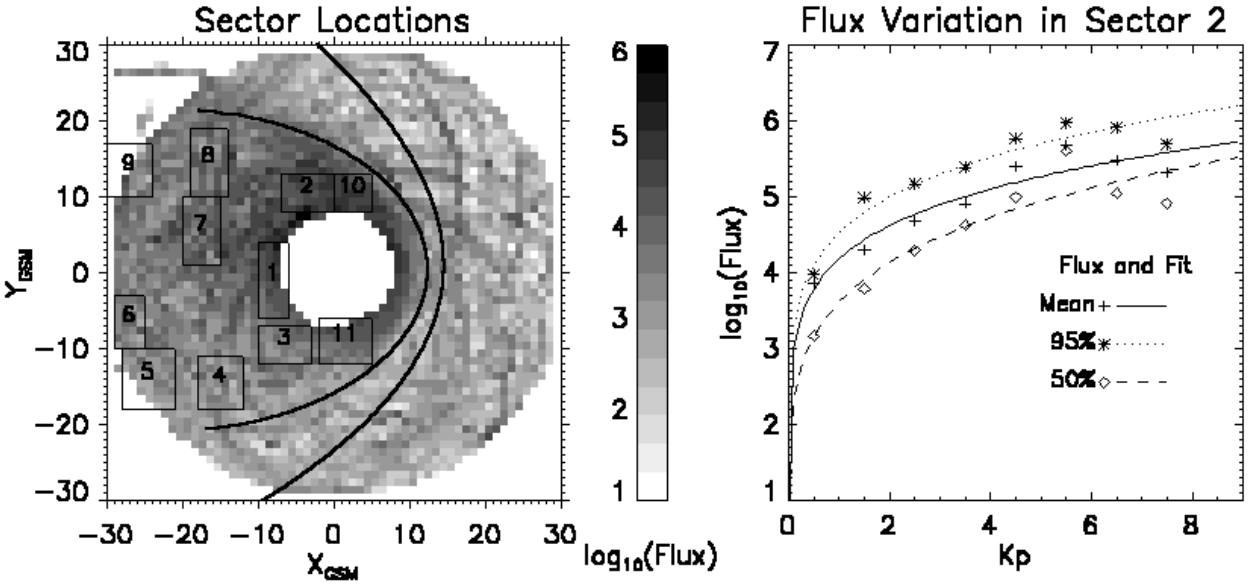

Figure 5. Flux Scaling. Sectors are identified in (a) that were used to obtain scaling laws for the flux (in units of protons/[cm^2-sec-sr-MeV]) as a function of Kp. The flux variation as a function of Kp is given in (b) for Sector 2. Statistics of the flux variation for each Kp level is determined to provide a basis for estimating the probability of encountering extreme flux values and a method of scaling statistically significant scaling flux distributions at low Kp to the poor statistics in the high Kp cases.

Scaling laws used for each Kp interval are calculated at the spacecraft's current location by finding the distance weighted sum of the N closest sectors. The objective of the distance scaling is to arrive at a set of Kp scaling factors which have been "blended" together according to their relative distances from the point at which output is desired. The first step is to multiply the closest sector's Kp scaling factors by the distance to the farthest sector. The next step is to multiply the second closest sector's Kp scaling factors by the distance to the second farthest sector. This process is repeated until the farthest sector's Kp scaling factors are multiplied by the distance to the closest sector. The final set of Kp scaling factors are found by summing the distance scaled quantities and dividing the sum by the total distance to all of the sectors.

The average flux at the center of each Kp interval is calculated next. A nearest-neighbor approach is used to obtain the spacecraft's flux in units of ions/[cm^2-sec-sr-MeV]) along its orbit. Constraints in the allowed Z-coordinates of database cells are used to assure that only cells within a predefined Z range from the spacecraft location are used defining the ion flux. The nearest data cell to the spacecraft location is found that lies within the layer of Z_{GSM} values in which the spacecraft currently resides. Boundaries of the layers are found for Z_{GSM} values of -7, -6, -5, +4, +5, +6, +7, +8, +9, +10, and +11R_E. For example, if the point has a Z_{GSM} value of 5.5 R_E,, the nearest-neighbor data cell is found which lies between +5 and +6 R_E. If the point is below –6 R_E, the near-neighbor data cell is found that lies between –7 and –6 R_E. If the point in question is above +10 R_E, then the near-neighbor is found that lies between +10 and +11 R_E. A number of other parameters are computed in addition to the flux. These parameters include the average number of flux data elements used to obtain the flux, the distance to the center of the nearest data cell used for the flux computation, and the number of flux database cells used that fall within the range tolerance to the nearest-neighbor cell (range tolerance value is currently set to 0.1 R_E). This additional information is computed so that flux values in different Kp intervals can be used to arrive at a composite flux prediction for the current Kp value (after Kp scaling of each interval's flux). The final value for the flux is determined by calculating the weighted sum (average) of all of the useable flux values that lie within the specified range tolerance above the minimum range (currently set to 1 R_E). The flux statistics (i.e., mean, 50%, 95% levels) are derived by multiplying the average flux value at the spacecraft's location by the distance weighted sum of the Kp scaling factors.

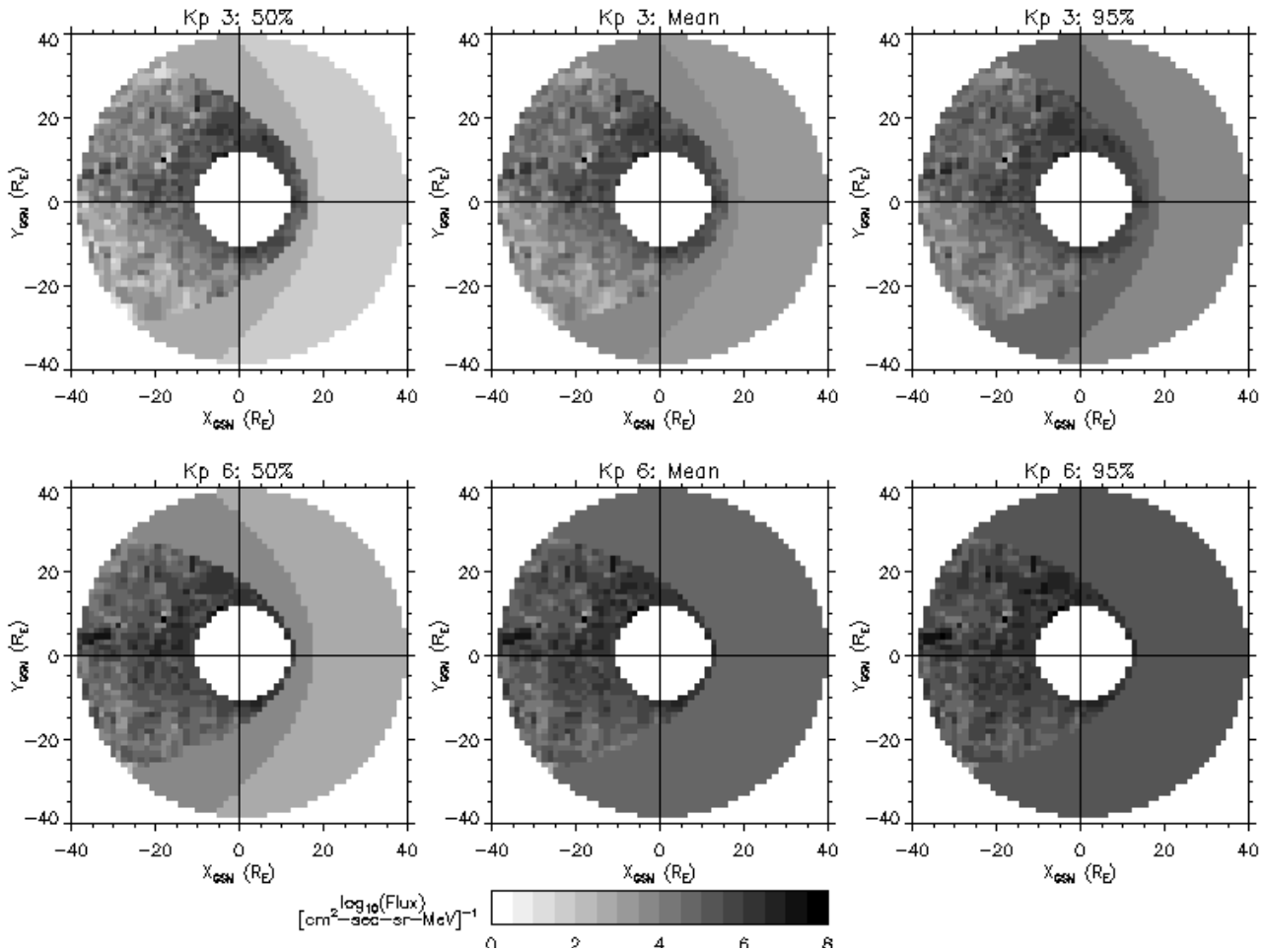

Figure 6. Example CRMFLX Model Results. Model output for 100 keV to 200 keV protons at the 50%, Mean, and 95% statistical levels are presented for geomagnetic disturbance levels of Kp 3 and Kp 6. The dawn-dusk flux asymmetry within the outer magnetosphere is provided by the model as well as increasing flux in the magnetosheath.

4. MODEL RESULTS

Examples of the scaled model output projected onto the X-Y_{GSM} plane are given in Figure 6 where the 50%, mean, and 95% results are presented for Kp 3 and Kp 6 conditions. Proton flux is greatest in the dusk sector ($Y_{GSM}>0$, $X_{GSM}\approx 0$) where the 100 keV to 200 keV ions are driven by the combined effects of magnetic curvature and gradient B forces. This asymmetry, absent in the azimuthally symmetric AP-8 model, is an important factor for the CXO because the satellite will encounter flux variations in the outer magnetosphere throughout the year due to the varying orientation of the magnetosphere relative to the orbit fixed in inertial space. Orbits passing through the midnight through dusk sectors, currently the summer and fall months, will encounter the greatest ion fluxes during the year. Conversely, orbits in the daytime through dawn sectors, currently the winter and spring months, will encounter minimum ion flux. The model does not contain any information on flux for radial distances less than approximately 9 R_E due to the limitation of the *Geotail* EPIC/ICS database. This is not considered to be a limitation for the CXO program as it is almost certain the ACIS instrument is unlikely to ever be used at smaller radial distances.

There are no spatial flux variations in both the magnetosheath and solar wind in the current version of the CRMFLX model. Although uniform values were assumed for computational efficiency, there is a marked increase in flux as a function of both statistical level and Kp. Future versions will include flux variations in the sheath and solar wind although an option is provided in the current version of the code for the user to provide solar wind flux from satellite measurements.

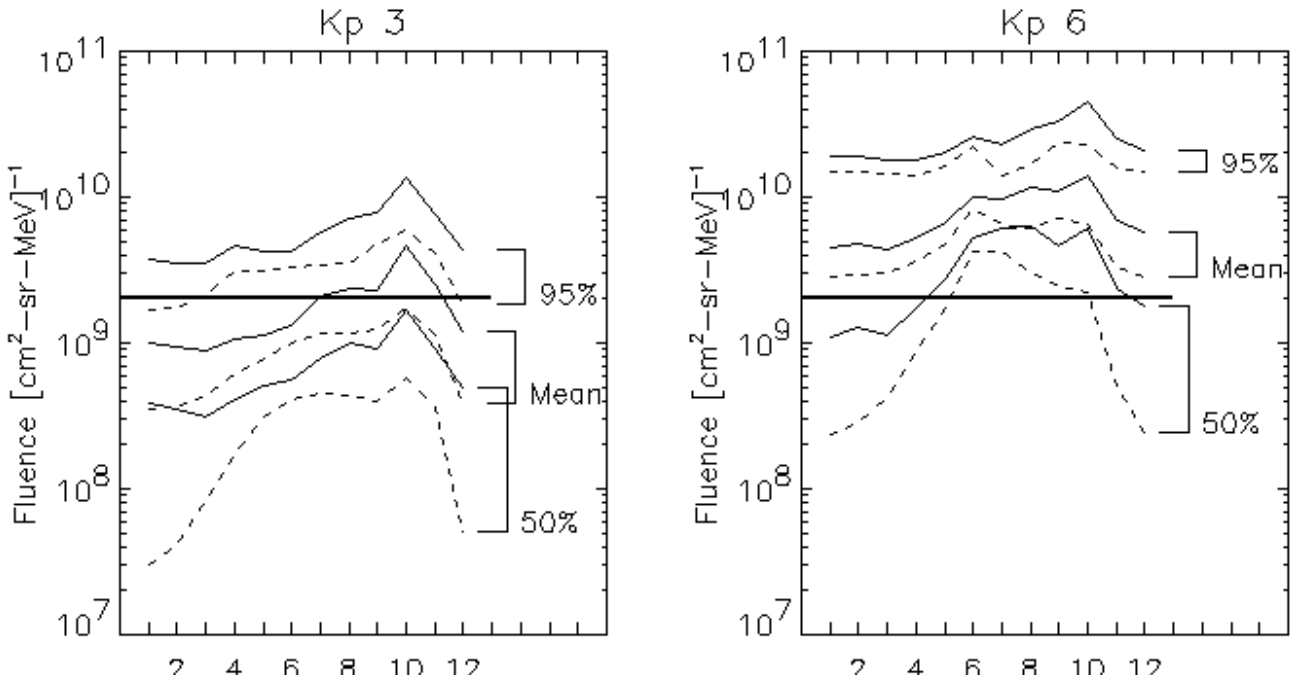

Figure 7. Average Fluence per Orbit for the Year 2000. Examples of the ion fluence along the CXO orbit are given for radial distances beyond 9 Re (solid) and 13 Re (dash) for the 50%, mean, and 95% ion model results. The dark horizontal line at a fluence of $2x10^9$ protons/[cm^2-sr-MeV] marks the approximate fluence value per orbit that will meet the targeted ACIS 5% CTI increase per year.

Estimates of the average free field fluence per orbit while the ACIS detector is exposed to the space environment is given in Figure 7 for the year 2000. Ion fluence is obtained by integrating the flux along the satellite orbit for all radial distances above a fixed value where the ACIS detector is assumed to be moved out of the focal plane and into a protected position. A solid line marks the fluence adopted by the *Chandra* team to meet the targeted 5% CTI increase for the ACIS detector per year. Figure 7 highlights the difference in proton fluence for different ACIS protection strategies if the detector is only in the focal plane above two different radial distances from the Earth. The pronounced peak during the late summer and autumn months is due to the orientation of the orbit in the magnetosphere during that time period. During this period the outbound leg of the orbit samples the magnetotail in the post-noon sector and the inbound leg the midnight to dusk sector, regions of the outer magnetosphere where ion flux is the most intense.

Limiting use of the detector at distances above 13 R_E assures the critical fluence is not exceeded in the 50% and mean environments for all months of the year under Kp=3 conditions. Only for the extreme 95% case does CRMFLX predict fluences in excess of the critical value for Kp=3 conditions. Under disturbed Kp=6 conditions the situation is quite different, the model shows that the critical fluence per orbit can be exceeded during the summer and fall months of the year for each of the 50%, mean, and 95% environments. However, Kp≥6 conditions are rare events and therefore the overall contribution to the accumulated ion fluence over long periods need not be large.

Examination of the CRMFLX fluence curves for use of ACIS at radial distance above 9 R_E shows there is a higher risk of accumulating fluences greater than the critical level. For example, in the Kp=3 case even the mean model predicts the proton fluence per orbit to exceed the critical level during the months of July through November. The mean and 95% environments exceed the critical flux for all months of the year for disturbed Kp=6 conditions.

CRMFLX Kp dependent flux output can be used with tables of Kp statistics by mission planners to predict the magnitude of flux and fluence along CXO orbits for periods up to many weeks ahead of time, a requirement for scheduling upcoming observing events. For example, Figure 8 shows a histogram of Kp values for a period of time covering over three solar cycles. The mean Kp value for this time period is 2.3, suggesting the Kp=3 results in Figure 7 for fluence per orbit represent greater than mean conditions based on past history of solar and geomagnetic activity. However, it is important to note that the average ion flux environment is not the mean Kp but rather more like $\ln_2(<2^{KP}>)$ because flux is an exponential function of Kp.

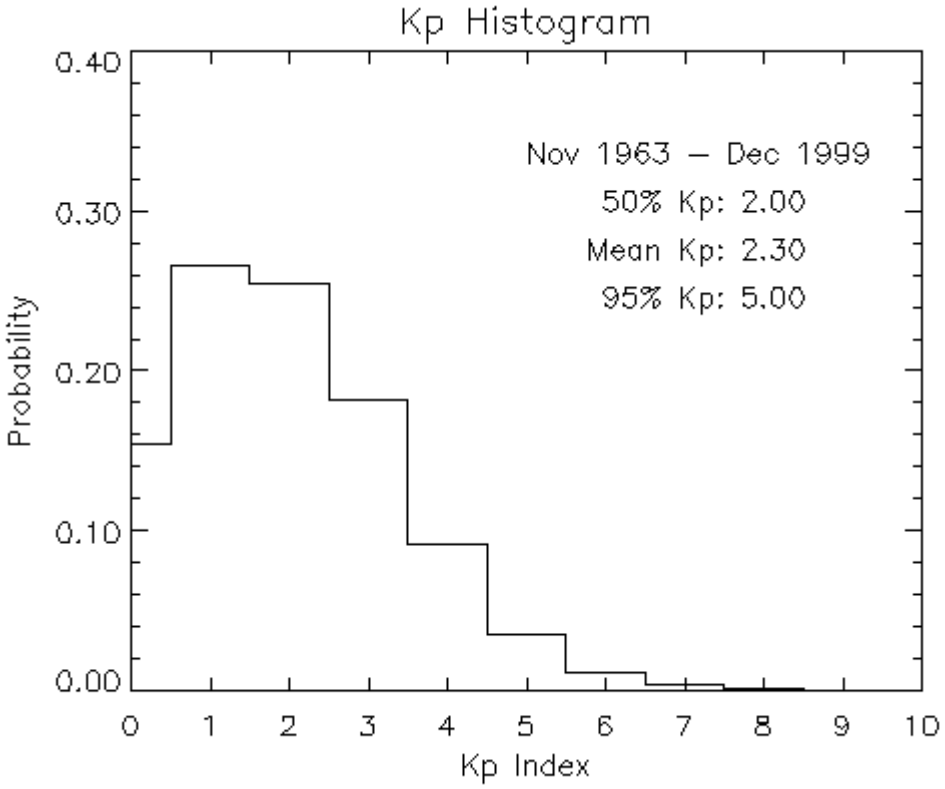

Figure 8. Kp Statistics. The histogram includes data from November 1963 through December 1999, an interval which includes over three complete solar cycles. The most probable value is Kp=1.7 for the complete set of data. The Kp=3 fluence plot shown in Figure 7 is therefore indicative of greater than mean conditions if the phase of the solar cycle is not considered.

Further analysis of the Kp record to include binning of the data by sunspot number, 10.7 cm radio flux, or other proxy of solar activity may provide a useful method of applying the model to predict flux variations as a function of phase in solar cycle.

The model is currently being incorporated into the OFLS software for scheduling on-orbit events based on 100-200 keV proton flux and fluence in addition to the current orbit events which include radiation belt entry/exit based on AP-8, sun-moon exclusion angles, and other significant environmental factors. An additional use of the model is for real time estimates of flux along the satellite orbit and accumulated proton fluence for intervals when ACIS is in the focal plane. The *Chandra* Flight Operations Team has recently implemented a version of the code in their space environment monitoring software that is available for the satellite operators in making operation decisions during periods of high geomagnetic activity.

5. SUMMARY

We have developed an engineering model of the ion flux in the outer magnetosphere for radial distances between 9 R_E and 30 R_E. The empirical model provides predictions of ion flux as a function of geomagnetic activity at user requested locations in the model domain. Output of the model is ion flux (currently only protons although He and CNO is in the process of being added) and identification of plasma regime as magnetosphere, magnetosheath, or solar wind. The flux model is based on data from the EPIC/ICS instrument onboard the *Geotail* satellite through the interval from 1995 through 2000. Experimental versions of the code are in the process of being incorporated into the OFLS software for scheduling on-orbit events for the CXO mission. The *Chandra* Operations team has also incorporated the code into real-time software for use in monitoring flux and fluence along the satellite orbit.

ACKNOWLEDGMENTS

Dr. Richard McEntire and Mr. Stuart Nylund (JHU/APL) provided *Geotail* EPIC/IPS data. Mr. Tom Guffin, Mr. Bill Davis, and Dr. Bill Cooke (CSC) provided the CXO ephemeris information. We obtained geomagnetic indices from the NSSDC OMNIWeb at NASA/GSFC. *Geotail* CPI/Hot Plasma Analyzer data plots were provided courtesy of Dr. Louis Frank and Dr. William R. Paterson, University of Iowa. We wish to thank Mr. Steve Smith (CSC) for his help in assembling the database and providing computer support. SNV acknowledges support for this work from NASA contract NAS8-39073. WCB, JIM, and KMW were supported by NASA Contract NAS8-40836 to Sverdrup Technology, Inc.

REFERENCES

1. Kolodziejczak, J.J., R. F. Elsner, R. A. Austin, and S. L. O'Dell, "Ion transmission to the focal plane of the Chandra X-Ray Observatory", these proceedings.
2. O'Dell, S.L., M.W. Bautz, W.C. Blackwell, R.A. Cameron, R.F. Elsner, M.S. Gussenhoven, J.J. Kolodziejczak, J.I. Minow, D.A. Swartz, A.F. Tennant, S.N. Virani, and K. Warren, "Radiation environment of the Chandra X-Ray Observatory", these proceedings.
3. Prigozhin, G.Y., M.W. Bautz, C. Grant, S. E. Kissel, B. LaMarr, and G.R. Ricker, Jr., "Characterization of the radiation damage in the Chandra X-ray CCD's", these proceedings.
4. Prigozhin, G.Y., S.E. Kissel, M.W. Bautz, C. Grant, B. LaMarr, R.F. Foster, G.R. Ricker, and G.P. Garmire, "Radiation damage in the Chandra X-ray CCD's", in *X-Ray Optics, Instruments, and Missions*, Proc. SPIE, 4012, edited by J. Trumper and B. Aschenbach, pp. 720 – 730, 2000.
5. Fairfield, D.H., "Average and unusual locations of the Earth's magnetopause and bow shock", *J. Geophys. Res*., 76, 6700 - 6717, 1971.
6. Krimigis, S.M., D.G. Sibeck, and R.W. McEntire, "Magnetosphere particle injection and the upstream ion event of September 5, 1984", *Geophys. Res. Lett*., 13, 1376 -1379, 1986.
7. Sibeck, D.G., R.W. McEntire, A.T.Y. Lui, S.M. Krimigis, L.J. Zanetti, and T.A. Potemra, "The magnetosphere as a source of energetic magnetosheath ions", *Geophys. Res. Lett.* 14, 1011 - 1014, 1987.
8. Sawyer, D. and J. Vette, "AP-8 trapped proton environment for solar maximum and solar minimum", National Space Science Data Center, Report 76-06, Greenbelt, Maryland, 1976.
9. Gaffey, J. and D. Bilitza, "NASA/National Space Science Data Center trapped radiation models", *J. Spacecraft and Rockets*, 31, 172, 1994.
10. Virani, S.N., R. Muller-Mellin, P.P. Plucinsky, and Y.M. Butt, "The Chandra X-Ray Observatory's radiation environment and the AP-8/AE-8 model", in *X-Ray Optics, Instruments, and Missions III, Proc. SPIE*, 4012, edited by J. Trumper and B. Aschenbach, pp. 669 – 680, 2000.
11. Fung, S.F., "Recent development in the NASA trapped radiation models", in *Radiation Belts: Models and Standards*, Geophysical Monograph 97, edited by J.F. Lemaire, D. Heynderickx, and D.N. Baker, American Geophysical Union, Washington, D.C., pp. 79 – 91, 1996.
12. Armstrong, T.W., and B.L. Colborn, "Trap/SEE Code Users manual for Predicting Trapped Radiation Environments", NASA CR-2000-209879, Marshall Space Flight Center, January, 2000.
13. Williams, D. J., R. W. McEntire, C. Schlemm II, A. T. Y. Lui, G. Gloeckler, S. P. Christon, and F. Gliem, "Geotail energetic particles and ion composition instrument," *J. Geomag. Geoelect*., 46, 39-57, 1994.
14. Frank, L. A., K. L. Ackerson, W. R. Paterson, J. A. Lee, M. R. English and G. L. Pickett, "The Comprehensive Plasma Instrumentation (CPI) for the Geotail Spacecraft", *J. Geomag. and Geoelectr*., 46, 23-37, 1994.
15. Karanikola, I., G.C. Anagnostopoulos, and A. Rigas, "Characteristics of 290 keV magnetosheath ions", *Ann. Geophys*., 17, 650, 1999.
16. Anagnostopoulos, G.C., G. Argyropoulos, and G. Kaliabetsos, "Spatial distribution of upstream magnetospheric 50 keV ions", *Ann. Geophys*., 18, 42, 2000.
17. Tsyganenko, N.A., "A magnetospheric magnetic field model with a warped tail current sheet", *Planet. Space Sci*., 37, 5 – 20, 1989.
18. Tsyganenko, N.A. "Modeling the Earth's magnetospheric magnetic field confined within a realistic magnetopause", *J. Geophys.Res*., 100, 5599-5612, 1995.
19. Bennett, L., M. G. Kivelson, K. K. Khurana, L. A. Frank, and W. R. Paterson, "A model of the Earth's distant bow shock", *J. Geophys. Res.*, 102, 26927 – 26941, 1997.
20. Mayaud, P.N., *Derivation, Meaning, and Use of Geomagnetic Indices*, Geophysical Monograph 22, American Geophysical Union, Washington, D.C., 1980.